An activatable biphotonic lanthanide probe for detection of nitroreductase in live bacteria and cancer cells

Carolina S. Vinagreiro[#1], Qian Liu[#2], Qinghua Wang[2], Xiang Wang [2], Hai-Yu Hu*[2] and Marc Nazaré*[1]

[1] Leibniz-Forschungsinstitut für Molekulare Pharmakologie Berlin (FMP), Medicinal Chemistry, 13125 Berlin, Germany, E-mail: nazare@fmp-berlin.de

[2] Institute of Materia Medica (IMM); Chinese Academy of Medical Sciences & Peking Union Medical College, Beijing, China, E-mail: haiyu.hu@imm.ac.cn

Abstract

We describe a nitroreductase activatable lanthanoid-based turn-on probe for two-photon imaging. The terbium-based luminescent probe is non-fluorescent in its inactive state but can be selectively activated by nitroreductase, leading to the release of the sensitizing antenna that facilitates energy transfer to the lanthanide center, resulting in an intense luminescence signal. We show the probe's capability to selectively sense nitroreductase not only in bacterial lysates but also in live bacteria of the ESKAPE family. Moreover, the probe effectively detects mammalian nitroreductase in prostate cancer cells, which is expressed under mild hypoxic conditions. The results obtained set the stage for a new generation of activatable lanthanoid-based probes that are suitable for two-photon excitation.

Introduction

Optical imaging tools contribute significantly to the deciphering of complex biological processes. Furthermore, beyond this, they are now also an indispensable technique in medical diagnostics for rapid, non-invasive, real-time monitoring of pathological processes ranging from the molecular level to whole organisms. Lanthanide complexes have been widely explored in this

context due to their exceptional fluorescent features in comparison with organic fluorophores, such as long luminescence lifetimes, high photostability, large Stokes shift, simple tuning of the emission wavelengths from visible to near-infrared and fingerprint emission bands.[1, 2] In particular, when put in combination with two-photon excitation microscopy, lanthanide probes offer several advantages for the noninvasive imaging of biological systems.[3, 4] Two-photon excitable lanthanide luminescent probes combine the unique f-element spectroscopic properties with the intrinsic advantages of nonlinear two-photon excitation, making them particularly attractive for bioimaging applications. The shifted excitation in the near-infrared spectral range largely reduces photo bleaching and photo-damage, and furthermore allows for high-contrast, high-resolution deep-tissue imaging, thereby avoiding commonly encountered limitations such as light attenuation, autofluorescence, and scattering are minimized.[5, 6] However, effective excitation of the lanthanide requires an organic chromophore as a sensitizing antenna, which in turn enables energy transfer, as well as surmounts the Laporte-forbidden f–f transitions and the resulting low extinctioncoefficient.[1, 7, 8] Bioresponsive activatable lanthanoid probes have been previously investigated by us as well as others using caged antenna precursors.[8-14] Such probes are turned on when in contact with the analyte, which triggers the sensitizing antenna. This offers substantial advantages over traditional always-on probes, due to their inherently increased sensitivity that results from the triggered signal amplification alongside the strongly reduced background signal. While sensitization of lanthanides luminescence using two-photon excitation was established over a decade ago,[15, 16] it is only recently that elegant studies have been conducted using two-photon excitable lanthanide luminescent probes for bioimaging applications. [17-26]

However, activatable bioresponsive two-photon excitable lanthanide luminescent probes have surprisingly not been investigated so far to the best of our knowledge, and reports on activatable carbostyril antennas remain scarce.[10]

As part of our program investigating nitroreductase (NTR) probes, [10, 27-29] we were particularly interested in the design and development of a DOTA-based two-photon excitable lanthanide luminescent probe for the detection of nitroreductase. NTRs are a family of flavin-containing bacterial enzymes, which catalyze the reduction of nitro functional groups and other nitrogen-

containing functionalities in the presence of NADH or NADPH as a cofactor.[30] They are present in bacterial pathogens, namely in multidrug-resistant members of the ESKAPE family (*Acinectobacter baumannii, Pseudomonas aeruginosa, Staphylococcus aureus, Enterococcus faecium, Klebsiella pneumonia*, and *Escherichia coli*), and are responsible for the vast majority of healthcare-associated bacterial infections. Moreover, NTRs are overexpressed in hypoxic cancer cells.[31] Hypoxia is a feature common in most solid tumors and a key determinant of cancer growth and propagation.[32, 33] Consequently, sensing hypoxic cancer cells could lead to efficient early detection of tumors and thus more favorable clinical outcomes.[34, 35] However, although NTRs are potentially highly relevant diagnostic markers for the detection of bacterial infections[29, 36, 37] and tumor cells[38-42], activatable lanthanide-based probes that take advantage of the favorable features of lanthanide luminescence still remain rarely exploited.[10]

Herein, we describe the first robust enzyme-responsive lanthanoid-based luminescent probe using two-photon excitation for the highly selective detection of nitroreductases in live bacteria and cancer cells. This terbium-based two-photon excitable probe is (1) simple to synthesize; (2) gives a turn-on emission over zero background; (3) is highly sensitive, selective, and stable; (4) is able to selectively detect nitroreductases in live bacteria of the ESKAPE family, as well as in live prostate cancer cells in mild hypoxic environments.

Results and discussion

Design of the probe. The general design strategy for the construction of our NTR-responsive two-photon excitable turn-on probe was to employ a non-sensitizing caged antenna precursor that, upon reaction with the enzyme, triggers a fragmentation cascade and releases the antenna. This in turn then enables the energy transfer to the lanthanide center upon two-photon excitation (Scheme 1). A prerequisite for establishing a DOTA-based two-photon turn-on probe is the availability of a robust non-sensitizing caged antenna precursor and an efficient energy transfer to the lanthanoid upon enzyme-triggered release of the antenna.

Although carbostyrils are well-known antennas for sensitization of different lanthanides, they have barely been exploited under two-photon excitation.[15, 43] We hypothesized that 7-aminocarbostyrils would be a suitable antenna for the envisioned two-photon excitation and

could lead to an efficient energy transfer for the lanthanide. Upon NTR-mediated reduction of the nitro group of the *para*-nitrobenzylcarbamate to the corresponding aniline, a spontaneous and irreversible disassembly of the linker would be induced, releasing the 7-aminocarbostyril sensitizing antenna. This design concept is highly modular, as a potentially new analyte can be made detectable simply by varying the trigger moiety of the enzymatically cleavable cage.

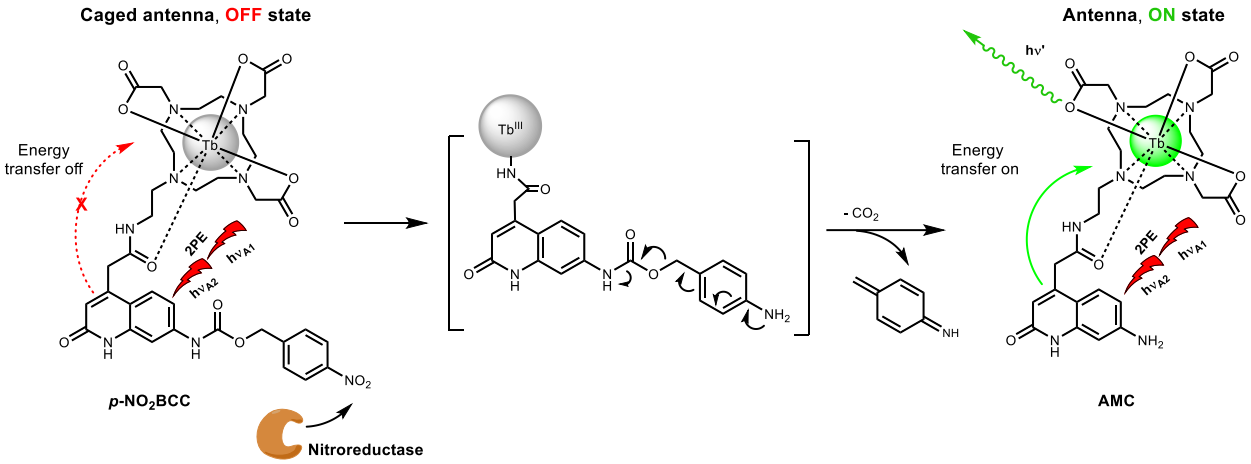

Scheme 1. Design and mode of action of our activatable biphotonic lanthanide probe for detection of nitroreductases.

Theoretical Calculations. To further support this hypothesis, we carried out time-dependent density functional theory (TD-DFT) calculations, using the caged *p*-NO_2benzylcarbamatecarbostyril (***p*-NO$_2$BCC**) and the activated 7-aminocarbostyril (**AMC**) antennas as simplified models. The emission intensities are primarily determined by the molar absorptivity of the $S_0 \rightarrow S_1$ transition of the antenna, the efficiency of intersystem crossing (ISC) between the antenna excited states and the $T_1 \rightarrow {}^5D_J$ energy transfer between antenna and lanthanide.[44-47]As shown in Table S1, **AMC** exhibits an oscillator strength of 0.23 for the S_1 excited state, indicating a significant molar absorptivity of the $S_0 \rightarrow S_1$ transition of the antenna. Moreover, the energy gap of the $T_1 \rightarrow {}^5D_4$ transition of **AMC** is 0.428 eV, which is sufficiently large to minimize back-energy transfer (ΔE ≥0.229 eV).[48] The high molar absorptivity of the $S_0 \rightarrow S_1$ transition together with a favorable energy gap between $T_1 \rightarrow {}^5D_4$ predicted an efficient energy transfer to the lanthanide, which should consequently enable a pronounced luminescence emission of the uncaged probe. Moreover, the installation of the NTR activatable *para*-nitrobenzylcarbamate

should cage the chromophoric unit according to our DFT calculations and provide a non-fluorescent, self-immolative NTR sensitive trigger moiety. The DFT calculations indicated that the LUMO+1 and HOMO of ***p*-NO$_2$BCC** are predominantly resident on the carbostyril part, while the LUMO and HOMO-3 are situated on the *p*-nitrobenzylcarbamate acceptor section (Figure 1a). In this case, the excited state of the fluorophore transfers electrons to the acceptor's LUMO, leading to fluorescence quenching through a d-PET mechanism.[49] In addition, the energy gap of the $T_1 \rightarrow {}^5D_J$ transition for the caged antenna ***p*-NO$_2$BCC** is very small (0.015 eV), leading to efficient back-energy transfer between the antenna and the lanthanide (Table S1). These results indicated that there was an efficient intended suppression of any lanthanoid luminescence by the caging characteristics of the ***p*-NO$_2$BCC** antenna precursor.

To support the envisioned TPA properties of probe **8,** we conducted a computational study of the **AMC** system at the SAOP/DZP level.[50] The TPA-simulated profile is represented in Figure 1b, and the theoretical imaginary part of the third-order hyperpolarizability (γ^{TPA}) and TPA cross section (σ^{TPA}), a quantitative measure of the probability of the two-photon absorption, are summarized in Table S2. The results show that our probe exhibits high TPA cross section values (σ^{TPA}> 500G) within a wavelength range of 640-720 nm. These values are in the range of the best two-photon absorption cross-sections described for lanthanide ligands and related complexes[51-61] and are far higher than for most organic dyes[62] or endogenous chromophores found in biological media[63]. These results suggested a very promising suitability of our probe for two-photon microscopy.

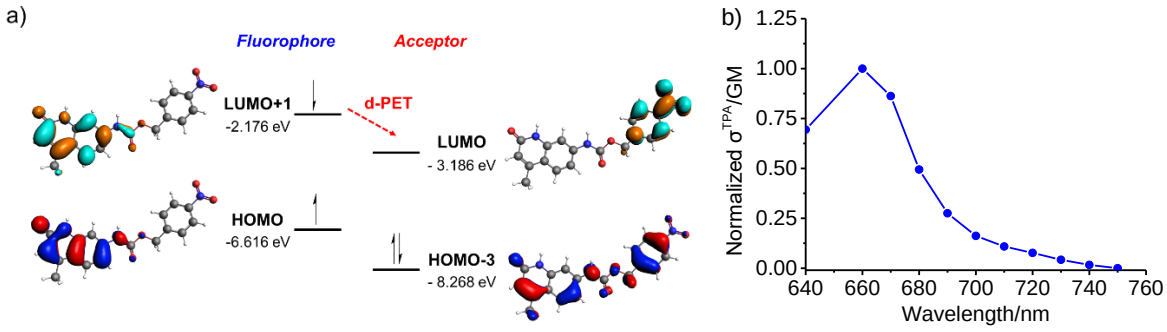

Figure 1. a) Frontier molecular orbital energy levels and electron density of HOMO-3/HOMO/LUMO/LUMO+1 of fluorophore of ***p*-NO$_2$BCC.** b) Theoretical two-photon absorption profile of ligand of **AMC** computed at the SAOP/DZP level.

Synthesis of the probe. The caged probe precursor **6** and the probe **8** were prepared in a short, high-yielding synthesis shown in Scheme 2. Firstly, the 7-aminocarbostyril antenna **2** was synthesized starting from 3-phenylenediamine **1,** followed by the introduction of the *para*-nitrobenzylcarbamate cage moiety. Deprotection of the acid group of the carbostyril antenna allowed the attachment of **4** to the asymmetricallysubstituted DOTA moiety[64] via amide coupling. Key intermediate **5** was then obtained after cleavage of the *tert*-butyl groups with 4M HCl in dioxane. This conjugate **5** was used directly to prepare the Tb(III) caged probe **6** and the uncaged 7-aminocarbostyril **7**. This circumvented the chemoselectivity issues encountered in the amide coupling step when unprotected 7-aminocarbostyril was used instead of *para*-nitrobenzylcarbamate acid **4**. The uncaging was performed using 2M NaOH at 50°C under strict control of short reaction times, affording **7** in 51% yield. Terbium complexation to the final compounds **6** and **8** was then accomplished by reaction with Terbium(III) trifluoromethane sulfonate in HEPES buffer.

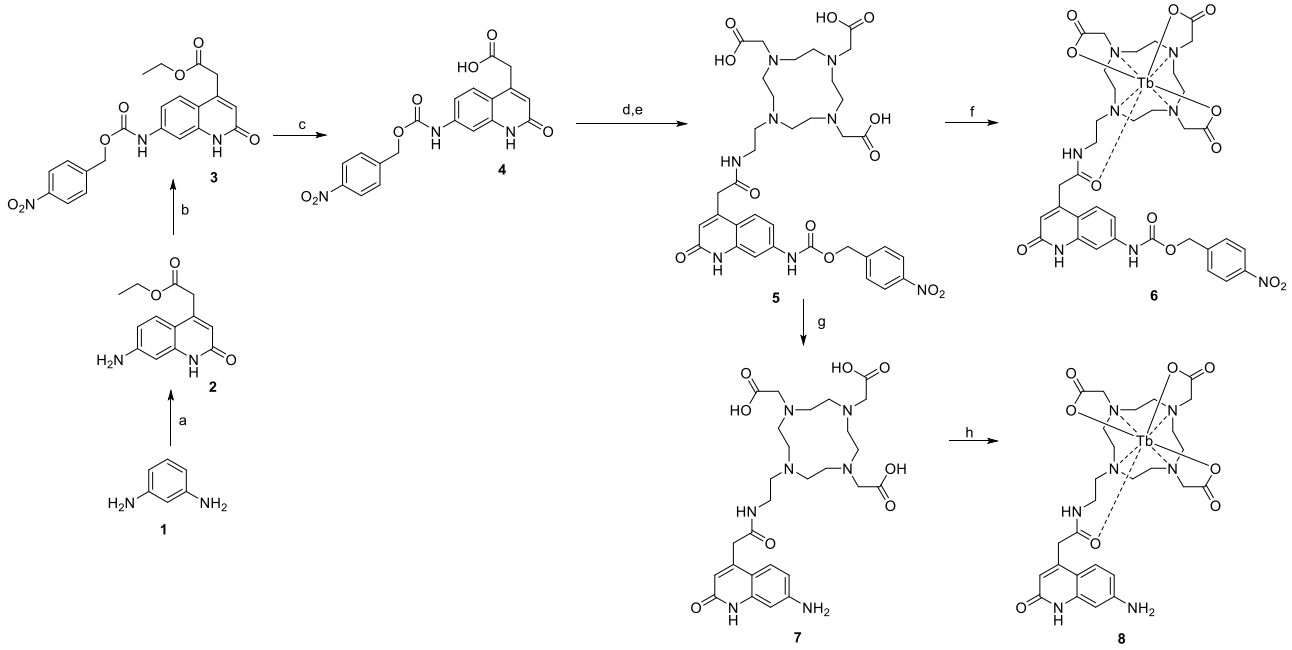

Scheme 2. Synthesis of activatable luminescent probe and respective activated probe. a) Diethyl-1,3-acetonedicarboxylate, $ZnCl_2$, DMSO, 100 °C, 20 h, 60%. b) 4-Nitrobenzyl chloroformate, pyridine, DMF, 0-25 °C, 18 h, 65%. c) Lithium hydroxide, DMF/water, 25 °C, 18 h, 53%. d) EDC:HCl, HOBt, 1-(2-ethylamine)-4,7,10-tris(tert-butoxycarbonylmethyl)-1,4,7,10-tetraazacyclotetradecane, DMF, 18 h. e) 4M HCl in dioxane, 50 °C, 18 h, 80% (2 steps). f) Tb(III) trifluoromethane sulfonate, HEPES buffer, 18 h, 45 %. g) 2M NaOH, methanol, 50 °C, 2 h, 51%. h) Tb(III) trifluoromethane sulfonate, HEPES buffer, 18 h, 42%.

Photophysical characterization.

The spectroscopic absorption, excitation, and fluorescence properties of probes **6** and **8** were determined in Tris-HCl buffer at pH 7.4 (Figure 2a). The caged probe **6** and activated control **8** showed absorption maxima at 330/344 and 346 nm, respectively. The excitation spectra were similar to their absorption spectra, confirming terbium sensitization by the antenna. Caged probe **6** was essentially non-emissive when excited at 345 nm, while the activated probe **8** displayed intense lanthanide luminescence under time-resolved conditions (75 µs), which confirms the predicted characteristics of the DFT calculations.

The total luminescence quantum yield of probe **8** was determined to be 1.92%, which is amongst the best values for turn-on luminescent probes featuring an analyte-triggered antenna formation.[10]

In addition, the two-photon-excited emission spectra of probe **8** at different incident intensity in 0.05 M Tris-HCl buffer (pH 7.4) were measured (Figure S1d, ESI†). As shown in Figure 2b, the fitted slope between integrated fluorescence intensity and pulse intensity was 2.0, which follows the square-law dependent intensity at low excitation.[65]

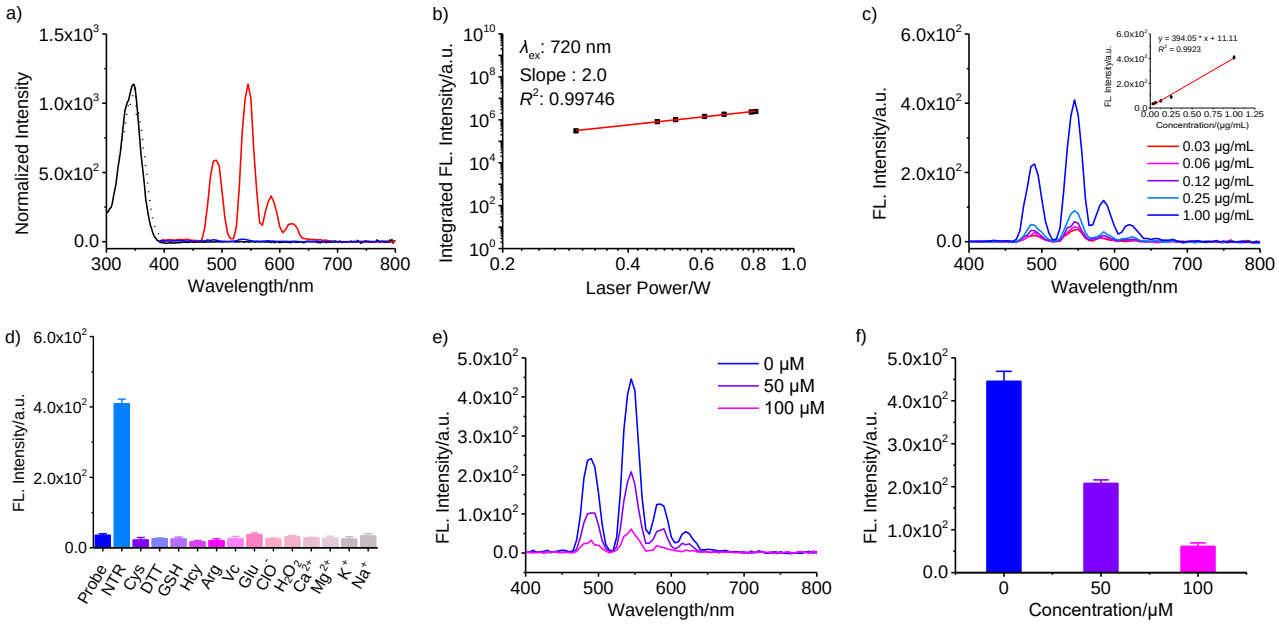

Figure 2. a) Normalized absorption (black), excitation (monitored at 545 nm, dotted black), and time-resolved fluorescence spectra of activated probe **8** (75 µs delay, red) and time-resolved fluorescence spectrum of caged probe **6** (75 µs delay, blue), each 20 µM in 0.05 M Tris-HCl buffer (pH 7.4); b) Plots of

integrated fluorescence intensity of two-photon-excited fluorescence emission spectra of probe **8** (50 μM) versus laser power. The excitation wavelength is 720 nm and the pulse width is about 140 fs. c) Time-resolved fluorescence spectra of caged probe **6** (20 μM) upon titration with different concentrations of NTR (0.03125, 0.0625, 0.125, 0.25, 1.0 μg/mL) in 0.05 M Tris-HCl buffer (pH 7.4) containing 50 μM NADH at 37 °C for 2 h. Inset: Linear correlation between NTR concentration and emission intensity at 545 nm, 75 μs delay, λ_{ex} = 345 nm. d) Fluorescence responses of caged probe **6** (20 μM) to various species in 0.05 M Tris-HCl buffer (pH 7.4) after 2 h incubation at 37 °C (λ_{ex} = 345 nm; λ_{em} = 545 nm; delay time: 75 μs): NTR (1 μg/mL), Cys (1 mM), DTT (1 mM), GSH (1 mM), Hcy (1 mM), Arg (1 mM), Vc (1 mM), glucose (10 mM), NaClO (10 mM), H_2O_2 (10 mM), $CaCl_2$ (2.5 mM), $MgCl_2$ (2.5 mM), KCl (10 mM), and NaCl (10 mM); e) The fluorescence emission spectra and f) fluorescence intensity (λ_{em} = 545 nm) of caged probe **6** (20 μM) in the enzyme reaction with different concentrations of inhibitor dicoumarin were collected at the excitation wavelength of 345 nm. As buffer medium 0.05 M Tris-HCl (pH 7.4) including 1.0 μg/mL nitroreductases and 50 μM NADH was used.

Probing nitroreductase.

Next, we exposed caged probe **6** to NTR analyte to investigate its ability to detect NTR *in vitro* on a biochemical level (Figure 2c). Upon successive increases of NTR concentration (upon 1 μg/ml) in the presence of NADH (50 μM), the emission intensities gradually increased, achieving a 12.5-fold signal increase with 1 μg/ml NTR (Figure 2c). Moreover, we studied the effect of temperature and pH on the conversion reaction of caged probe **6** in the presence of NTR (Figures S3 and S4, ESI†), which confirmed that physiological conditions are the optimal conditions for detection (pH 7.4 and 37 °C). Under these optimized conditions, time-resolved luminescence titrations at 545 nm showed that the probe response to NTR was linear in the 0.03125−1 μg/ml [NTRs] range (R^2 = 0.9923, Figure 2c). The detection limit ($3\sigma/k$) was calculated to be at 8 ng/mL NTR. σ is the standard deviation (S.D.) of the measured fluorescence intensities of caged probe **6** (20 μM) without NTR at 545 nm. k is the slope of the linear regression equation. The rate of the uncaging reaction of **6** to probe **8** triggered by NTR was measured and the apparent kinetic parameters K_m and V_{max} were determined to be 51.55 μM and 0.025 μM/s, respectively (see Figure S4, ESI†), which were comparable to previous values reported for NTR.[66]

Given the analyte complexity of the intracellular environment, we next assessed the specificity and stability of the caged probe **6** for the precise detection of NTR activity in the presence of high concentrations of various common bioanalytes. This is important to exclude undesired interfering

background reactions induced by species such as thiols (Cys, DTT, GSH and homocysteine-HCy), arginine (Arg), ascorbic acid (Vc), glucose (Glu), reactive oxygen species (NaOCl, H_2O_2) and inorganic salts ($CaCl_2$, $MgCl_2$, KCl and NaCl) in a cellular setting. As shown in Figure 2d, incubation of the caged probe **6** with all these analytes evoked no response, including reductive thiols at high concentrations. In stark contrast, a strong luminescence signal was observed in this setting when caged probe **6** was incubated in the presence of NTR. This luminescent response to NTR could be abolished in a concentration manner by preincubation with dicoumarine[67], a known NTR inhibitor. A concentration-dependent luminescence decrease confirmed the triggered activation of our probe by a specific NTR-catalyzed reduction reaction (Figures 2e and f).

Detection of NTR in bacterial lysates

We then investigated the ability of the caged probe **6** to detect NTR in bacterial lysates. In order to obtain further insight, six strains of the ESKAPE panel were selected comprising five Gram-negative *K. pneumoniae*, *E. faecium*, *A. baumannii*, *P. aeruginosa,* and *E. coli,* as well as one Gram-positive *S. aureus*. The bacteria (OD_{600} = 10) were lysed by ultrasonication in the ice bath and were then centrifuged at 4 °C. The supernates were incubated with or without dicoumarin inhibitor for 2 h and subsequently with probe **6** for another 2 h before recording the emission signal at 545 nm. Probe **6** was particularly strongly activated in *K. pneumoniae* and *E. coli,* while the activation was less pronounced in the other strains (Figures 3a and b). The different responses could be attributed to different NTR expression levels in combination with different species of the enzyme itself due to the low conservation throughout these strains, as well as species dependent disparities in the intracellular permeation of the caged probe **6**.[29] A pronounced reduction of the luminescent signal intensity was observed upon the addition of NTR-inhibitor dicoumarin to the bacterial culture before treatment with the probe, again confirming the specificity of the probe **6** towards intracellular NTR activation.

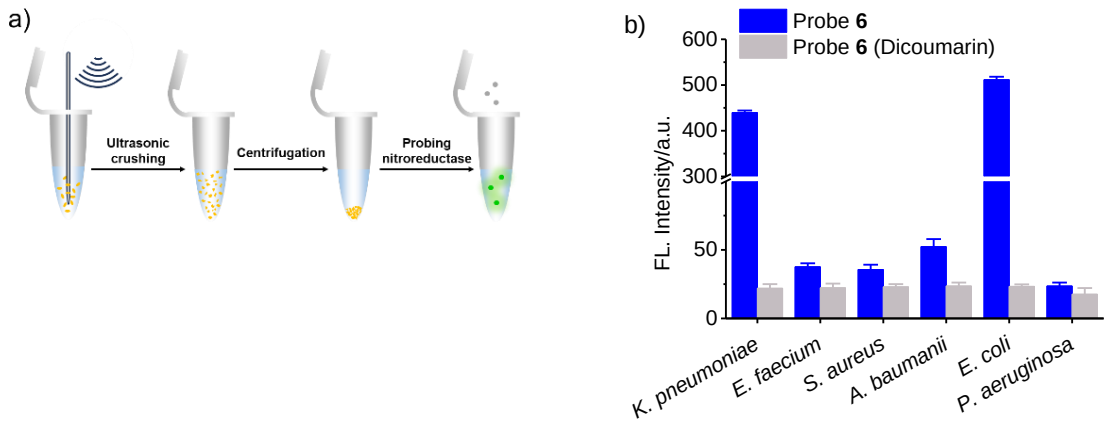

Figure 3. a) Diagram of cell lysate extraction process; b) Fluorescence intensity of caged probe **6** (20 μM) activated by nitroreductase in bacteria lysate of the ESKAPE panel with or without dicoumarin (100 μM) (OD_{600} = 10; λ_{ex} = 345 nm; λ_{em} = 545 nm; delay time: 75 μs).

Bacterial imaging using two-photon excitation

Subsequently, we investigated whether our probe was able to detect NTR in live bacteria under two-photon excitation (λ_{ex} = 720 nm) using confocal microscopy. We observed that caged probe **6** was able to be activated in *K. pneumoniae* and *E. coli* after apparent intracellular uptake, showing a strong fluorescence signal at 550 nm (Figures 4a and b). The activation of the probe was attenuated by the presence of the NTR-inhibitor dicoumarin, where only faint fluorescence was observed (Figures 4c and S7b, S8 SI†), thereby illustrating NTR-specific activation. While the caged probe **6** was readily taken up by bacteria, the activated probe **8** was barely able to permeate into bacterial cells and only a very weak fluorescence signal was observed (see Figure 4d and Figure S6a, ESI†). Overall, these results indicate enhanced intracellular enrichment of activated probe **8** due to lower permeability, which further contributes to localization, signal amplification and contrast.

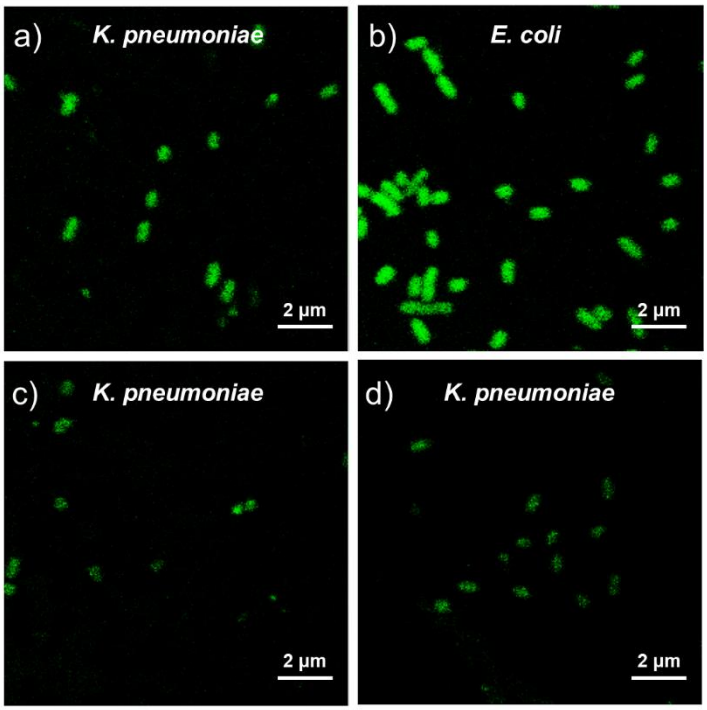

Figure 4. The fluorescence imaging after incubating with a) Caged probe **6** (50 μM) in *K. pneumoniae*; b) Caged probe **6** (50 μM) in *E. coli;* c) Caged probe **6** with 100 μM dicoumarin in *K. pneumoniae* and d) activated probe **8** (50 μM) in *K. pneumoniae* in 0.05 M Tris-HCl (pH 7.4) for 2 h at 37 °C (λ_{ex} = 720 nm, λ_{em} = 550 nm, scale bar = 2 μm).

Fluorescent imaging of hypoxic cells. NTRs are overexpressed in hypoxic cancer cells, making them a target for cancer detection. To investigate if our probe was suitable to be activated under these conditions in mammalian cells, we selected prostate cancer cells PC-3 that are susceptible to hypoxia.[68] The hypoxic environment for the cells was induced by limiting the oxygen supply to 1% oxygen during cell culture, which is considered mild hypoxic conditions. Subsequently, the PC-3 cells were incubated with caged probe **6** under normoxic and hypoxic conditions, and were monitored by confocal two-photon microscopy. In the case of hypoxic PC-3 cells, strong fluorescence was observed at 550 nm, in stark contrast to the faint fluorescence observed under normoxic conditions (Figures 5a, b and d). We also tested the activated probe **8** under the same hypoxic conditions and observed a much less pronounced fluorescence signal compared to caged probe **6** (Figure 5c and d).

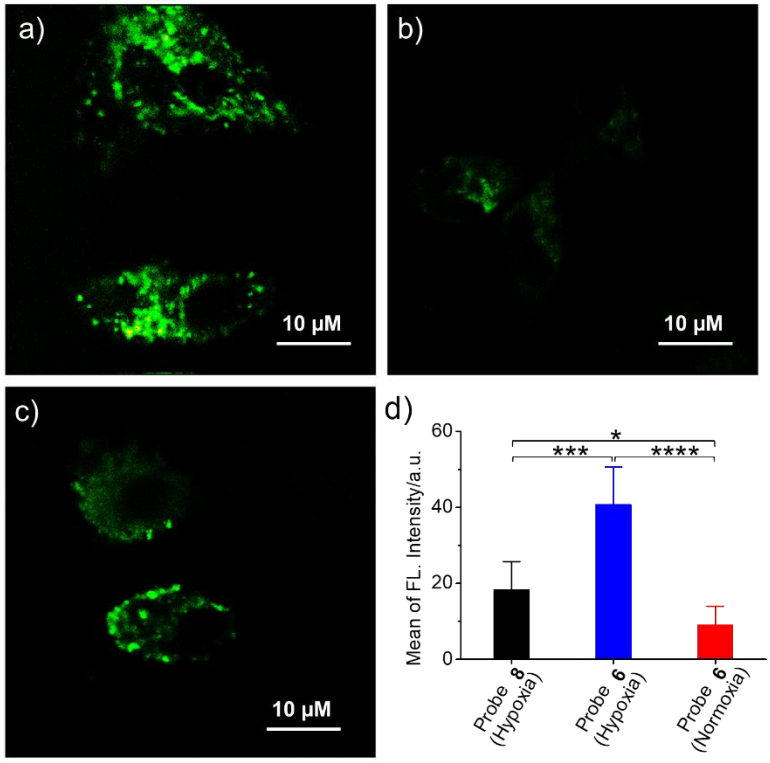

Figure 5. The fluorescence imaging of prostate cancer cells PC-3 after 2 h incubating with a) Caged probe **6** (50 μM) in a hypoxia environment (5% CO_2, 1% O_2); b) Caged probe **6** (50 μM) in a normal environment (5% CO_2); and c) Activated probe **8** (50 μM) in a hypoxia environment (5% CO_2, 1% O_2) (λ_{ex} = 720 nm, λ_{em} = 550 nm, scale bar =10 μm); d) Calculated mean fluorescence intensity of fluorescence imaging of by ImageJ.

Conclusion

In summary, we have developed the first versatile and robust enzyme activatable two-photon excitable lanthanoid-based fluorescent probe for the selective detection of nitroreductases. Construction of a new and simple caged carbostyril-based enzyme responsive antenna moiety permitted access to an essentially non-sensitizing antenna precursor, which, upon release, is suitable for two-photon excitation. We demonstrated that our probe is able to selectively sense NTR in lysates and in live bacteria. Using confocal fluorescence microscopy under two-photon excitation, we observed efficient intracellular uptake and activation in bacteria of the highly clinically relevant multi-resistant pathogens ESKAPE family, which are responsible for the majority of hospital infections. Moreover, the probe allowed detection of prostate cancer cells by two-photon fluorescence imaging, even in a mild hypoxic environment. These results show for

the first time how the enzyme activatable lanthanoid-based fluorescent probe can be applied in live bacteria and cancer cell detection, and may pave the way for novel diagnostic modalities in medical applications.

Acknowledgements

The authors are grateful to Marta Diceglie, Sandra Miksche and Peter Lindemann for HRMS measurements, Peter Schmieder and the NMR core facility for analytical compound characterization, the Screening Unit for access to equipment and Barth van Rossum for graphical artwork (all Leibniz-Forschungsinstitut für Molekulare Pharmakologie (FMP)). We thank Sascha Eidner and Thomas Schwarze (both University of Potsdam) for their support and helpful discussions. We thank Mingxing Chen (PKU)，Jing Li (CAS) and Dr. Yuansheng Sun (ISS) for their kind support and valuable discussions. This work was in part funded by the Sino-German research project PAGODA by the Federal Ministry of Education and Research (BMBF) under Grant No. 01DO22001A.

References

1. M. C. Heffern, L. M. Matosziuk and T. J. Meade, *Chem. Rev.*, 2014, **114**, 4496-4539.
2. D. Parker, *Chem. Soc. Rev.*, 2004, **33**, 156-165.
3. W. Denk, J. H. Strickler and W. W. Webb, *Science*, 1990, **248**, 73-76.
4. M. Göppert-Mayer, *Ann. Phys.*, 1931, **401**, 273-294.
5. P. T. So, C. Y. Dong, B. R. Masters and K. M. Berland, *Annu. Rev. Biomed. Eng.*, 2000, **2**, 399-429.
6. M. Pawlicki, H. A. Collins, R. G. Denning and H. L. Anderson, *Angew. Chem. Int. Ed. Engl.*, 2009, **48**, 3244-3266.
7. A. Thibon and V. C. Pierre, *Anal. Bioanal. Chem.*, 2009, **394**, 107-120.
8. S. H. Hewitt and S. J. Butler, *Chem. Commun.*, 2018, **54**, 6635-6647.
9. R. Gui, H. Jin, X. Bu, Y. Fu, Z. Wang and Q. Liu, *Coord. Chem. Rev.*, 2019, **383**, 82-103.
10. B. Brennecke, Q. Wang, Q. Zhang, H.-Y. Hu and M. Nazaré, *Angew. Chem. Int. Ed.*, 2020, **59**, 8512-8516.
11. E. Pershagen and K. E. Borbas, *Angew. Chem. Int. Ed.*, 2015, **54**, 1787-1790.
12. E. Pershagen, J. Nordholm and K. E. Borbas, *J. Am. Chem. Soc.*, 2012, **134**, 9832-9835.
13. C. Szíjjártó, E. Pershagen, N. O. Ilchenko and K. E. Borbas, *Chem. - Eur. J.*, 2013, **19**, 3099-3109.
14. A. R. Lippert, T. Gschneidtner and C. J. Chang, *Chem. Commun.*, 2010, **46**, 7510-7512.
15. M. H. V. Werts, N. Nerambourg, D. Pélégry, Y. L. Grand and M. Blanchard-Desce, *Photochem. Photobiol. Sci.*, 2005, **4**, 531-538.
16. L.-M. Fu, X.-F. Wen, X.-C. Ai, Y. Sun, Y.-S. Wu, J.-P. Zhang and Y. Wang, *Angew. Chem. Int. Ed.*, 2005, **44**, 747-750.

17. A. Picot, A. D'Aléo, P. L. Baldeck, A. Grichine, A. Duperray, C. Andraud and O. Maury, *J. Am. Chem. Soc.*, 2008, **130**, 1532-1533.
18. F. Kielar, A. Congreve, G.-l. Law, E. J. New, D. Parker, K.-L. Wong, P. Castreño and J. de Mendoza, *Chem. Commun.*, 2008, **21**, 2435-2437.
19. M. Soulié, F. Latzko, E. Bourrier, V. Placide, S. J. Butler, R. Pal, J. W. Walton, P. L. Baldeck , B. Le Guennic, C. Andraud, J. M. Zwier, L. Lamarque, D. Parker and O. Maury, *Chem. - Eur. J.*, 2014, **20**, 8636-8646.
20. S. V. Eliseeva, G. Auböck, F. van Mourik, A. Cannizzo, B. Song, E. Deiters, A.-S. Chauvin, M. Chergui and J.-C. G. Bünzli, *J. Phys. Chem. B.*, 2010, **114**, 2932-2937.
21. N. Hamon, A. Roux, M. Beyler, J.-C. Mulatier, C. Andraud, C. Nguyen, M. Maynadier, N. Bettache, A. Duperray, A. Grichine, S. Brasselet, M. Gary-Bobo, O. Maury and R. Tripier, *JACS*, 2020, **142**, 10184-10197.
22. H. Li, R. Lan, C.-F. Chan, G. Bao, C. Xie, P.-H. Chu, W. C. S. Tai, S. Zha, J.-X. Zhang and K.-L. Wong, *Chem. Commun.*, 2017, **53**, 7084-7087.
23. J. Mendy, A. Thy Bui, A. Roux, J.-C. Mulatier, D. Curton, A. Duperray, A. Grichine, Y. Guyot, S. Brasselet, F. Riobé, C. Andraud, B. Le Guennic, V. Patinec, P. R. Tripier, M. Beyler and O. Maury, *ChemPhysChem*, 2020, **21**, 1036-1043.
24. V. Placide, A. T. Bui, A. Grichine, A. Duperray, D. Pitrat, C. Andraud and O. Maury, *Dalton Trans.*, 2015, **44**, 4918-4924.
25. C. Andraud and O. Maury, *Eur. J. Inorg. Chem.*, 2009, **2009**, 4357-4371.
26. Y. Ma and Y. Wang, *Coord. Chem. Rev.*, 2010, **254**, 972-990.
27. L. Zhang, Y. Liu, Q. Zhang, T. Li, M. Yang, Q. Yao, X. Xie and H. Y. Hu, *Anal. Chem.*, 2018, **90**, 1934-1940.
28. Y. Liu, L. Zhang, M. Nazare, Q. Yao and H.-Y. Hu, *Acta Pharm. Sin. B.*, 2018, **8**, 401-408.
29. S. Xu, Q. Wang, Q. Zhang, L. Zhang, L. Zuo, J.-D. Jiang and H.-Y. Hu, *Chem. Commun.*, 2017, **53**, 11177-11180.
30. M. D. Roldán, E. Pérez-Reinado, F. Castillo and C. Moreno-Vivián, *FEMS Microbiol. Rev.*, 2008, **32**, 474-500.
31. E. Akiva, J. N. Copp, N. Tokuriki and P. C. Babbitt, *PNAS*, 2017, **114**, E9549-E9558.
32. S. Kizaka-Kondoh, M. Inoue, H. Harada and M. Hiraoka, *Cancer Sci.*, 2003, **94**, 1021-1028.
33. A. L. Harris, *Nat. Rev. Cancer*, 2002, **2**, 38-47.
34. J. M. Brown and W. R. Wilson, *Nat. Rev. Cancer*, 2004, **4**, 437-447.
35. C. J. Koch and S. M. Evans, *Semin. Nucl. Med.*, 2015, **45**, 163-176.
36. Y. Ji, Y. Wang, N. Zhang, S. Xu, L. Zhang, Q. Wang, Q. Zhang and H.-Y. Hu, *JOC*, 2019, **84**, 1299-1309.
37. Z. Zhang, T. Lv, B. Tao, Z. Wen, Y. Xu, H. Li, F. Liu and S. Sun, *Bioorg. Med. Chem.*, 2020, **28**, 115280-115286.
38. Y.-L. Qi, L. Guo, L.-L. Chen, H. Li, Y.-S. Yang, A.-Q. Jiang and H.-L. Zhu, *Coord. Chem. Rev.*, 2020, **421**, 213460-213485.
39. R. S. Boddu, O. Perumal and D. K, *Biotechnol. Appl. Biochem.*, 2021, **68**, 1518-1530.
40. S. Sarkar, H. Lee, H. G. Ryu, S. Singha, Y. M. Lee, Y. J. Reo, Y. W. Jun, K. H. Kim, W. J. Kim and K. H. Ahn, *ACS Sens.*, 2021, **6**, 148-155.
41. J.-n. Liu, W. Bu and J. Shi, *Chem. Rev.*, 2017, **117**, 6160-6224.
42. D. Yang, H. Y. Tian, T. N. Zang, M. Li, Y. Zhou and J. F. Zhang, *Sci. Rep.*, 2017, **7**, 9174-9182.
43. G. Piszczek, B. P. Maliwal, I. Gryczynski, J. Dattelbaum and J. R. Lakowicz, *J. Fluoresc.*, 2001, **11**, 101-107.
44. C. M. G. dos Santos, A. J. Harte, S. J. Quinn and T. Gunnlaugsson, *Coord. Chem. Rev.*, 2008, **252**, 2512-2527.

45. C. P. Montgomery, B. S. Murray, E. J. New, R. Pal and D. Parker, *Acc. Chem. Res.*, 2009, **42**, 925-937.
46. J.-C. G. Bünzli, *Acc. Chem. Res.*, 2006, **39**, 53-61.
47. J.-C. G. Bünzli and S. V. Eliseeva, in *Lanthanide Luminescence: Photophysical, Analytical and Biological Aspects*, eds. P. Hänninen and H. Härmä, Springer Berlin Heidelberg, Berlin, Heidelberg, 2011, pp. 1-46.
48. M. Latva, H. Takalo, V.-M. Mukkala, C. Matachescu, J. C. Rodríguez-Ubis and J. Kankare, *J. Lumin.*, 1997, **75**, 149-169.
49. W. Sun, M. Li, J. Fan and X. Peng, *Acc. Chem. Res.*, 2019, **52**, 2818-2831.
50. Z. Hu, J. Autschbach and L. Jensen, *J. Chem. Theory Comput.*, 2016, **12**, 1294-1304.
51. A. Bourdolle, M. Allali, A. D'Aléo, P. L. Baldeck, K. Kamada, J. A. G. Williams, H. Le Bozec, C. Andraud and O. Maury, *Chemphyschem*, 2013, **14**, 3361-3367.
52. M. Galland, T. Le Bahers, A. Banyasz, N. Lascoux, A. Duperray, A. Grichine, R. Tripier, Y. Guyot, M. Maynadier, C. Nguyen, M. Gary-Bobo, C. Andraud, C. Monnereau and O. Maury, *Chem. Eur. J.*, 2019, **25**, 9026-9034.
53. F. L. Jiang, W. K. Wong, X. J. Zhu, G. J. Zhou, W. Y. Wong, P. L. Wu, H. L. Tam, K. W. Cheah, C. Ye and Y. Liu, *Eur. J. Inorg. Chem.*, 2007, 3365-3374.
54. R. M. Pallares, M. Sturzbecher-Hoehne, N. H. Shivaram, J. P. Cryan, A. D'Aleo and R. J. Abergel, *J. Phys. Chem. Lett.*, 2020, **11**, 6063-6067.
55. M. Soulié, F. Latzko, E. Bourrier, V. Placide, S. J. Butler, R. Pal, J. W. Walton, P. L. Baldeck, B. Le Guennic, C. Andraud, J. M. Zwier, L. Lamarque, D. Parker and O. Maury, *Chem. - Eur. J.*, 2014, **20**, 8636-8646.
56. Q. Zhang, X. H. Tian, H. P. Zhou, J. Y. Wu and Y. P. Tian, *Materials*, 2017, **10**, 223-260.
57. M. H. V. Werts, N. Nerambourg, D. Pélégry, Y. Le Grand and M. Blanchard-Desce, *Photochem. Photobiol. Sci.*, 2005, **4**, 531-538.
58. A. T. Bui, A. Roux, A. Grichine, A. Duperray, C. Andraud and O. Maury, *Chem. Eur. J.*, 2018, **24**, 3408-3412.
59. A. T. Bui, M. Beyler, A. Grichine, A. Duperray, J.-C. Mulatier, Y. Guyot, C. Andraud, R. Tripier, S. Brasselet and O. Maury, *Chem. Commun.*, 2017, **53**, 6005-6008.
60. A. T. Bui, A. Grichine, S. Brasselet, A. Duperray, C. Andraud and O. Maury, *Chem. Eur. J.*, 2015, **21**, 17757-17761.
61. A. D'Aléo, A. Bourdolle, S. Brustlein, T. Fauquier, A. Grichine, A. Duperray, P. L. Baldeck, C. Andraud, S. Brasselet and O. Maury, *Angew. Chem. Int. Ed.*, 2012, **51**, 6622-6625.
62. N. S. Makarov, M. Drobizhev and A. Rebane, *Opt. Express*, 2008, **16**, 4029-4047.
63. W. R. Zipfel, R. M. Williams and W. W. Webb, *Nat. Biotechnol.*, 2003, **21**, 1369-1377.
64. E. Gianolio, R. Napolitano, F. Fedeli, F. Arena and S. Aime, *Chem. Comm.*, 2009, **40**, 6044-6046.
65. C. Xu and W. W. Webb, *J. Opt. Soc. Am. B*, 1996, **13**, 481-491.
66. H. Nivinskas, R. Koder, Ž. Anusevièius, J. Šarlauskas, A.-F. Miller and N. Čenas, *Acta Biochim. Pol.*, 2000, **47**, 941-949.
67. R. L. Koder and A.-F. Miller, *Biochim. Biophys. Acta, Protein Struct. Mol. Enzymol.*, 1998, **1387**, 395-405.
68. L. H. Higgins, H. G. Withers, A. Garbens, H. D. Love, L. Magnoni, S. W. Hayward and C. D. Moyes, *Biochim. Biophys. Acta Bioenerg.*, 2009, **1787**, 1433-1443.